TURKISH ENERGY, NUCLEAR AND MINERAL RESEARCH AGENCY
TURKISH JOURNAL OF NUCLEAR SCIENCES
E-ISSN: 2791-7185
https://dergipark.org.tr/tr/pub/tjns

# Preparation and characterization of various column-filling materials in order to optimize $^{68}$Ge-$^{68}$Ga generator column

**Elif Ekebaş Çavdar[1,*], Okan Oktar[1], Eren Çantay[1], Ece Ergun[1], Nur Banu Ertaş[1], Büşra Aydın[1], Özlem Abay[1]**

[1]*Turkish Energy, Nuclear and Mineral Research Agency, Nuclear Energy Research Institute, Ankara, Türkiye*

## ARTICLE INFO

**Article History:**
Received June 10, 2024
Available online July 15, 2024

**Research Article**

**Keywords:**
Adsorption
$^{68}$Ge/$^{68}$Ga generator
Inorganic adsorbent
Positron Emission Tomography (PET)
Radionuclide

## ABSTRACT

In order to obtain ready-to-use $^{68}$Ga in Positron Emission Tomography (PET) applications, the $^{68}$Ge/$^{68}$Ga generator system is an ideal source and allows PET imaging in centers without cyclotrons. In commercial generator systems, radiochemical separation of Ge (parent) and Ga (daughter) radionuclides is carried out in a generator column composed of inorganic adsorbents. In this study, commercially available tin oxide ($SnO_2$), laboratory-synthesized $SnO_2$, titanium oxide ($TiO_2$), and zeolite were used as column-filling materials. These column-filling materials, which are classified as inorganic adsorbents, were exposed to calcination process at two different temperatures. Their adsorption behaviors were investigated both prior to and following to the calcination. Ge and Ga were loaded on the columns to simulate the $^{68}$Ge/$^{68}$Ga generator system. They were eluted with different concentrations of HCl (0.01-1.5 M). All elemental analyses were performed using inductively coupled plasma mass spectrometry (ICP-MS). In addition, since the column-filling material and column used in the generator are exposed to radiation during the shelf life of the $^{68}$Ge/$^{68}$Ga generator, their radiation stability was also investigated. Structural characterization studies were performed with Fourier transform infrared spectroscopy (FTIR), Raman spectroscopy, and X-ray diffraction (XRD). In addition, the Brunauer-Emmett-Teller (BET) method was used to calculate the surface area and pore sizes of the column-filling materials. In the present work, Kw_$SnO_2$ calcined at 900 °C proved to be a promising sorbent.

## 1. Introduction

The development of the first radionuclide generators and the beginning of clinical applications date back more than 60 years. Although many parent/daughter radionuclide generator systems such as $^{188}$W/$^{188}$Re, $^{82}$Sr/$^{82}$Rb and $^{99}$Mo/$^{99m}$T have been investigated, only a few are currently used in routine research and clinical use. In recent years, the $^{68}$Ge/$^{68}$Ga generator system has played an important role in the medical field, as it is an alternative and excellent source to provide $^{68}$Ga in clinical positron emission tomography (PET) applications owing to its simplicity and convenience to use in any center without an on-site cyclotron [1-3].

The parent radionuclide, $^{68}$Ge, has a half-life of 270.8 days and is a positron emitter. Its physical properties allow one to use the generator for a long period, potentially over one year. The daughter radionuclide, $^{68}$Ga, with a physical half-life of 68 min, provides that $^{68}$Ga matches with small molecules and the pharmacokinetics of many peptides thanks to rapid diffusion, localization at the target, and fast blood clearances, all of which contribute to a low radiation dose for the patient [4]. Also, the applications of the generator based on $^{68}$Ga are used for not only the detection of molecular tumors, especially neuroendocrine tumors, targeting vectors such as proteins or peptides, but also the diagnosis of various cancers [3,5].

The working principle of these generators depends mainly on a chromatographic column to selectively separate the parent and daughter radionuclides. The parent radionuclide is adsorbed on column support materials, called an adsorbent, and the daughter radionuclide is subsequently and selectively eluted from the column using an elution agent while the parent radionuclide remains there. These column-filling materials have been developed over the years as either organic or inorganic, depending on $^{68}$Ga at an acceptable pH, the radioactive concentration, the acceptable breakthrough of $^{68}$Ge and the presence of potential metal ion impurities in the elution. Examples of $^{68}$Ge/$^{68}$Ga generator systems containing organic column-filling materials are cation and anion exchange materials based on the phenolic/N-methylglucamine group, silica derivates, and pyrogallol formaldehyde [1,2,6]. Thanks to their chemical stability and higher capacity, organic column-filling materials are the

*Corresponding author: elif.ekebascavdar@tenmak.gov.tr

most popular ion exchangers; however, some crucial properties, such as high selectivity and radiation stability on repeated elutions over a period, play an important role in these generator systems. Radiation stability reduces the capacity of organic materials with high selectivity. In addition, organic materials degraded by radiation reduce their chemical purity, which is especially important in the radiopharmaceuticals industry [1,6-9].

Inorganic adsorbents, on the other hand, have been developed for use in different areas of nuclear technology (such as the separation of fission products from spent fuel and deionization of reactor cooling water at high temperatures) thanks to their high radiation resistance compared to organic adsorbents [10]. In addition, inorganic ion exchangers can be customized to separate parent and daughter radionuclides with these properties under thermal and chemical conditions. Examples of $^{68}Ge/^{68}Ga$ generator systems with inorganic column-filling materials contains alumina ($Al_2O_3$), tin oxide ($SnO_2$), titanium oxide ($TiO_2$), cerium oxide ($Ce_2O$), and zirconium oxide ($ZrO_2$) adsorbents. In the commercial generators, $TiO_2$ and $SnO_2$ are used as inorganic column filling materials. These are available by Cyclotron Co. Ltd. (Russian Federation), Eckert & Zieger (Germany), Pars Isotope Company (Iran), and iThemba LABS (Republic of South Africa), respectively [4]. These inorganic adsorbents with a hydrated amorphous structure have some physical and chemical disadvantages. The physical and chemical deformation can cause the cracking of the column filling material, which blocks the flow of the daughter radionuclide during the elution process. Furthermore, cracking may also lead to the presence of potential metal ion impurities in the elution and the breakthrough of $^{68}Ge$ [4,10,11].

In this present work, to avoid the disadvantages of amorphous inorganic column-filling materials, the different inorganic adsorbents (such as $TiO_2$ and $SnO_2$) were exposed to the calcination process. For the structural characterization of the adsorbents, XRD, FTIR and Raman along with BET analysis were performed. The adsorption behaviors of adsorbents for the $^{68}Ge/^{68}Ga$ generator system were investigated using inductively coupled plasma mass spectrometry (ICP-MS) without the use of radioactive $^{68}Ge$.

## 2. Experimental

### *2.1.Materials*

All chemicals were used as received without further purification. The reagents, tin (II) chloride ($SnCl_2$) and glucose ($C_6H_{12}O_6$) purchased from Merck, ammonium carbonate ($(NH_4)_2CO_3$) from Honeywell, analytical grade reagents (metallic gallium, metallic germanium, and yttrium (99.999%), nitric acid ($HNO_3$, 37%), and hydrochloric acid (HCl, 65%) from Merck were used in this study. Deionized water from a Milli-Q ultrapure water system (Millipore Corp.) was used at all stages of the experiments. The zeolite, ZSM-5 ($SiO_2$/$Al_2O_3$) and titanium oxide (in the form of anatase) with particle sizes around 200 nm were supplied by Zeolyst (coded as ZSM-5) and Sigma Aldrich (coded as $TiO_2$), respectively. Titanium oxide powders in the form of anatase-rutile phase mixture or in the form of rutile phase were obtained by oven heating at 600 °C (coded as $TiO_2$-600) or at 900 °C (coded as $TiO_2$-900), respectively. The tin oxides were: $SnO_2$ synthesized with the mechanochemical method by Chakravarty [12] (coded as Gl_$SnO_2$) and $SnO_2$ nanopowder obtained by Sigma Aldrich (coded as Al_$SnO_2$). These tin oxides were exposed to calcination process at two different temperatures (coded as Gl_$SnO_2$_600, Gl_$SnO_2$_900, Al_$SnO_2$_600, and Al_$SnO_2$_900). In addition, tin oxide powder commercially available as high purity metastannic acid produced by Keeling & Walker were also studied either in as received form (Kw_$SnO_2$) or after heat-treatment (coded as Kw_$SnO_2$_600 and Kw_$SnO_2$_900). Kw_$SnO_2$_600 and Kw_$SnO_2$_900 coded powders were heat treated at 600 and 900 °C, respectively, for 3 hours in an electric furnace and left to cool down without temperature control All column-filling materials were sieved through a 150 µm mesh stainless steel sieve for efficient column operation [2,13].

### 2.2. Methods

#### *Determination of the distribution coefficient ($K_d$) of the Ge and Ga*

In order to separate Ga and Ge on the different column-filling materials, distribution coefficient ($K_d$) of Ge and Ga were investigated experimentally at different concentrations of hydrochloric acid (0.1M-1.5M HCl) under static conditions. 20 mL of different concentrations of HCl solution and about 200 mg of each column-filling material were added to each flask. 100 ppm stock Ge-Ga solution was prepared, and 0.1 mL of this stock solution was added to them (Fig. 1). The mixtures were shaken for 3 hours at room temperature and then filtered through a 0.45 µm Teflon filter. Aliquots of 5 mL were analyzed by ICP-MS. The $K_d$, expressed as ml/g, were calculated using the following expression [13,14]:

$$K_d = \frac{[C_{solid}]}{[C_{solution}]}$$

$[C_{solid}]$→concentration in the solid at equilibrium (µg/g)
$[C_{solution}]$→concentration in the solution at equilibrium (µg/ml)

#### *Determination of the adsorption capacity*

The adsorption capacity of column-filling materials was determined under static conditions. 10 mg of each column-filling material, 20 mL of different concentrations of HCl solution, and 0.1 mL of 100 ppm stock Ge-Ga stock solution were added to each flask.

**Figure 1.** Experimental setup used to determine $K_d$ under static conditions.

The mixtures were shaken for 3 hours at room temperature and filtered through a 0.45 um Teflon filter. Aliquots of 5 mL were analyzed by ICP-MS [2,13,14]. The adsorption capacities ($q_e$) of $Ge^{4+}$ in each of these inorganic adsorbents, expressed as mg/g, were calculated using the following expression:

$$q_e = \frac{V\,[C_0 - C_e]}{m}$$

$q_e \rightarrow$ the capacity of adsorbent (mg/g)
$C_0 \rightarrow$ the initial concentration of adsorbent (mg/L)
Ce $\rightarrow$ the final concentration of adsorbent (mg/L)
V $\rightarrow$ the volume of solutions (mL)
m $\rightarrow$ the mass (g) of the oxide

The $K_d$ results from static experiments may change under dynamic (column-flow) experimental conditions, so the same experiments were carried out under dynamic conditions using the columns representing the generator column [13].

### *Determination of the breakthrough of $Ge^{4+}$*

Using the experimental parameters (the concentration of HCl and the calcination temperature) determined under static experimental conditions, the possible breakthrough amount of $Ge^{4+}$ was examined under dynamic (column) experimental conditions was examined. Ge analysis in the eluate provided the key to the breakthrough of $Ge^{4+}$. The experimental setup prepared for the column studies is shown in Fig. 2.

The polypropylene (PP) columns (2.5 ml) with dimensions of 5×0.8×1.0 cm (height×inner diameter×outer diameter) with 10µm filters at the inlets and outlets were used in this study. The column was filled with 2 g of selected inorganic adsorbent and compressed in a vibrator to prevent any space between the particles. In order to remove possible small particles, the column was washed with 30 ml of hydrochloric acid with a peristaltic pump (0.25 ml/min). The stock Ge solution at different acid concentrations was loaded into the column. To observe a possible breakthrough of Ge from the column, it was washed with deonized water and HCl and then eluted with different concentrations of HCl. These eluates were analyzed by ICP-MS [13].

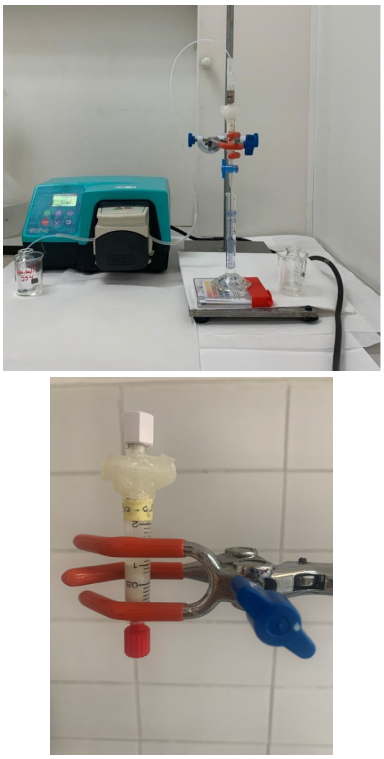

**Figure 2.** Experimental setup used to determine the breakthrough of Ge from column.

### *Characterization of inorganic adsorbents*

The inorganic adsorbents were characterized using different techniques in order to investigate their structures and properties. The characterizations were carried out using various analytical techniques such as FTIR, Raman spectroscopy, XRD and BET surface area analysis. The FTIR and Raman spectra of column-filling materials were recorded in the range of 525-4000 $cm^{-1}$ with the Thermo Nicolet 8700 FT-IR spectrometer and in the range of 101-3434 $cm^{-1}$ with the Thermo Scientific Nicolet Almega XR Dispersive Raman spectrometer, respectively. X-ray diffraction analysis of the samples were performed between angles 10°-80° (2θ) with Bruker D8 Advance X-ray Diffractometer operating at 40 kV and 30 mA using Cu-Kα radiation (λ = 1.5406 A°). The surface area and pore sizes of inorganic adsorbents were determined by the BET method using the Quantachrome brand AUTOSORB-1. Prior to analysis, 0.1-0.4 gram samples were degassed at 200 °C for 2 hours, and the specific surface area was determined by performing multi-point BET analysis with $N_2$ gas adsorption at liquid nitrogen temperature [13].

## 3. Results and discussion

### *Determination of the distribution coefficient ($K_d$) of the Ge and Ga*

The adsorption behavior of parent (Ga) and daughter (Ge) radionuclides on a particular adsorbent depends on the distribution coefficients of that radionuclide. The efficiency of radiochemical separation increases with

the difference between the distributions coefficients of two radionuclides. The amount of daughter radionuclide in the eluate (low $K_d$) should be high, and the breakthrough of parent radionuclide should be low in there. In this study, $K_d$ of Ga and Ge for each column-filling materials calcined at different temperatures were determined under static experimental conditions at eight different HCl concentrations.

For the 'Gl_$SnO_2$' heat treated samples, adsorption of Ga is higher at low acid concentrations (0.01 M HCl) at both calcination temperatures (Table 1). Gallium adsorption decreased following the increase in acid concentration. However, the distribution coefficient of Ge is very low indicating that Ge was not adsorbed by these column-filling materials [13].

**Table 1.** $K_d$ of Ge and Ga as a function of concentration of HCl for Gl_$SnO_2$.

| The concentration of acid (M) | Gl_$SnO_2$_600 | | Gl_$SnO_2$_900 | |
|---|---|---|---|---|
| | $K_d$ Ga | $K_d$ Ge | $K_d$ Ga | $K_d$ Ge |
| **0.01** | 996.5 | 203.4 | 1261.6 | 243.2 |
| **0.05** | 35.3 | 120.0 | 29.3 | 173.5 |
| **0.1** | 9.9 | 90.4 | 9.1 | 185.7 |
| **0.25** | 5.4 | 133.8 | 1.9 | 86.0 |
| **0.5** | 3.0 | 86.1 | 0.9 | 57.5 |
| **0.75** | 6.9 | 84.8 | 2.2 | 65.0 |
| **1.0** | 4.5 | 78.3 | 2.3 | 64.9 |
| **1.5** | 5.2 | 49.3 | 1.0 | 60.6 |

In Table 2, the $K_d$ of $SnO_2$ samples obtained from two different companies was calculated prior to calcination (Kw_$SnO_2$_nc and Al_$SnO_2$_nc) and after calcination at two different temperatures. In both samples, adsorptions of Ga were high at low acid concentrations (<0.05 M), regardless of the calcination temperature. While there was a dramatic decrease in the $K_d$ of Ga in both samples with increasing acid concentration, there was no significant decrease in the $K_d$ of Ge at 600°C and 900°C with increasing acid concentration (0.25 M<). These findings suggest that Ga has a noticeably lower $K_d$ than Ge, so it can separated from Ge.

The distribution coefficient of Ge and Ga for the commercially available 'ZSM-5' sample at different acid concentrations are given in Table 3. The $K_d$ of Ge and Ga for 'ZSM-5' was not as high as the $K_d$ value calculated for the other two commercial $SnO_2$ samples at eight different HCl concentrations.

$TiO_2$ has three types of crystallographic structures: anatase, rutile, and mixture of these two phases (anatase-rutile) (Table 4). The most stable phase is the rutile phase, while the anatase and mix anatase-rutile phases are metastable and unstable, respectively. Metastable phases of $TiO_2$ undergo phase transformation at high temperatures. The anatase phase transforms into the rutile phase above 700-800 °C [15]. Temperature-dependent phase transitions of $TiO_2$ directly affected the distribution coefficient of Ge

**Table 2.** $K_d$ of Ge and Ga as a function of HCl concentration for Kw_$SnO_2$ and Al_$SnO_2$ prior to calcination and after calcination at two different temperatures.

| The concentration of acid (M) | Kw_$SnO_2$_nc | | Kw_$SnO_2$_600 | | Kw_$SnO_2$_900 | |
|---|---|---|---|---|---|---|
| | $k_d$ Ga | $k_d$ Ge | $k_d$ Ga | $k_d$ Ge | $k_d$ Ga | $k_d$ Ge |
| **0.01** | 631.7 | 22525.0 | 84722.9 | 62921.0 | 45637.6 | 39846.4 |
| **0.05** | 555.5 | 20869.0 | 420.0 | 54610.8 | 241.0 | 40575.2 |
| **0.1** | 50.8 | 15470.9 | 68.1 | 39444.3 | 54.6 | 30131.6 |
| **0.25** | 13.7 | 2463.5 | 18.2 | 44121.7 | 8.0 | 23164.6 |
| **0.5** | 2.9 | 1552.6 | 1.2 | 38409.4 | 3.2 | 26658.4 |
| **0.75** | 0.3 | 1608.4 | 1.2 | 39290.1 | 3.5 | 22500.3 |
| **1.0** | 3.1 | 3130.0 | 4.9 | 43245.4 | 6.9 | 29368.6 |
| **1.5** | 17.7 | 2008.5 | 2.7 | 17813.7 | 8.8 | 12903.7 |

| The concentration of acid (M) | Al_$SnO_2$_nc | | Al_$SnO_2$_600 | | Al_$SnO_2$_900 | |
|---|---|---|---|---|---|---|
| | $K_d$ Ga | $K_d$ Ge | $K_d$ Ga | $K_d$ Ge | $K_d$ Ga | $K_d$ Ge |
| **0.01** | 20939.9 | 71502.3 | 31248.9 | 70133.5 | 26406.9 | 66926.9 |
| **0.05** | 260.0 | 67479.4 | 302.0 | 54723.8 | 326.7 | 60277.0 |
| **0.1** | 43.7 | 65510.2 | 47.1 | 63595.6 | 60.1 | 57218.3 |
| **0.25** | 7.4 | 61530.0 | 9.1 | 61397.4 | 10.9 | 50332.3 |
| **0.5** | 3.4 | 40812.9 | 3.7 | 59709.3 | 2.6 | 49159.3 |
| **0.75** | 3.4 | 68250.1 | 3.8 | 39579.9 | 10.2 | 47106.3 |
| **1.0** | 3.3 | 71421.5 | 6.6 | 75971.2 | 4.8 | 36435.7 |
| **1.5** | 4.5 | 33543.0 | 11.1 | 33797.9 | 9.1 | 30166.9 |

and Ga. At high calcination temperatures, the adsorption of Ge is extremely low. Samples calcined at 600 ºC showed a higher adsorption of Ge.

**Table 3.** $K_d$ of Ge and Ga as a function of concentration of HCl for ZSM-5.

| The concentration of acid (M) | ZSM-5 | |
|---|---|---|
| | $K_d$ Ga | $K_d$ Ge |
| **0.01** | 1442.0 | 5071.0 |
| **0.05** | 41.3 | 10965.8 |
| **0.1** | 26.6 | 11554.2 |
| **0.25** | 30.8 | 12478.4 |
| **0.5** | 36.4 | 14390.6 |
| **0.75** | 32.9 | 14603.4 |
| **1.0** | 40.5 | 16622.7 |
| **1.5** | 34.5 | 11949.9 |

The distribution coefficients of Ge and Ga calculated for different column-filling materials provide the determination of the acid concentration in the generator column, where Ge is adsorbed mostly and Ga can be eluted highly. In other words, the adsorption of Ge in the column matrix leads to high $K_d$, and the selective release of Ga in an acidic medium leads to low $K_d$ values.

The adsorption mechanism between adsorbent and Ge can be explained by the fact that the inorganic consist of discrete metal oxide clusters coated with surface hydroxyl groups. Between 0.01 M and 1.5 M HCl acid, pH decreases while acidity increases.

**Table 4.** $K_d$ of Ge and Ga as a function of HCl concentration of for $TiO_2$ prior to calcination and after calcination at two different temperatures.

| The concentration of acid (M) | $TiO_2$_nc | | $TiO_2$_600 | | $TiO_2$_900 | |
|---|---|---|---|---|---|---|
| | $K_d$ Ga | $K_d$ Ge | $K_d$ Ga | $K_d$ Ge | $K_d$ Ga | $K_d$ Ge |
| **0.01** | 158.2 | 8629.6 | 270.9 | 20926.9 | 162.5 | 359.9 |
| **0.05** | 4.3 | 3381.2 | 7.0 | 10832.0 | 5.8 | 246.2 |
| **0.1** | 3.3 | 2780.2 | 2.8 | 5701.4 | 2.4 | 146.4 |
| **0.25** | 1.1 | 1633.9 | 2.7 | 3902.5 | 1.3 | 108.0 |
| **0.5** | 5.0 | 845.0 | 6.0 | 2080.6 | 4.4 | 95.7 |
| **0.75** | 3.5 | 641.0 | 4.9 | 1650.3 | 4.2 | 81.5 |
| **1.0** | 4.6 | 503.8 | 2.0 | 1387.6 | 3.8 | 70.6 |
| **1.5** | 9.2 | 415.3 | 13.1 | 1107.0 | 10.6 | 78.8 |

At dilute acid concentrations (as pH increases), germanium hydroxide complexes become negatively charged i.e.$[GeO(OH)_3]^-$, $[GeO_2(OH)_2]^2$, and $[Ge(OH)_4]_8(OH)_3]^{3-}$ whereas the inorganic adsorbents have a positively charged surface and hence, great affinity for negatively charged Ge complexes due to their electrostatic attraction. In this mechanism, Ga exists as $Ga^{3+}$, and therefore, almost complete elution can be achieved due to the electrostatic repulsion between the positively charged $Ga^{3+}$ ion and the positively charged surface of the inorganic adsorbents [11].

### *Determination of the adsorption capacity*

Considering the calculated $K_d$, the adsorption capacities of Ge on the column-filling materials studied at different calcination temperatures and acid concentrations (HCl) gives information about how 1 gram of column-filling materials absorbs how many micrograms of Ge. The inorganic adsorbents with better $K_d$ values were selected and subsequently evaluated for their sorption capacity. According to the results, the suitable HCl concentrations for the $SnO_2$ samples calcined at 600 ºC and 900 ºC were determined as 0.05, 0.1, 0.25, and 0.5. Similarly, for $TiO_2$ calcinated at 600 ºC and ZSM-5adsorption capacity values were evaluated for the same HCl concentrations.

Table 5 shows the adsorption capacities of Ge on different column-filling materials. It is seen that the 'Kw_$SnO_2$' sample calcined at lower temperatures has a high Ge adsorption capacity, while the 'Al_$SnO_2$' sample calcined at two temperatures has a similar Ge adsorption capacity. Furthermore, examining the ZSM-5 $K_d$ values reveal unexpected results such that although there was not much difference between Ge and Ga affinities under static experimental conditions, ZSM-5 showed high adsorption capacity. This can be explained by the lattice structure of ZSM-5. Thanks to its cage structure, it does not separate Ga and Ge, but collapses Ge in the cage structure.

Therefore, to determine the breakthrough of $Ge^{4+}$ under dynamic experimental conditions, Al_$SnO_2$_900, Kw_$SnO_2$_600 and Kw_$SnO_2$_900 were eluted with 0.5 M HCl, while $TiO_2$_600 and ZSM-5 were eluted with 0.1 M HCl.

**Table 5.** The adsorption capacity of column-filling materials at different calcination temperatures with acid concentration.

| Column-filling materials | Calcination Temperatures | Acid Concentrations (M) | Micrograms that 1 g of column-filling materials can adsorb |
|---|---|---|---|
| **Kw_$SnO_2$** | 600°C | 0.05 | 613 |
| | | 0.1 | 640 |
| | | 0.25 | 540 |
| | | 0.5 | 533 |
| | 900°C | 0.05 | 501 |
| | | 0.1 | 475 |
| | | 0.25 | 426 |
| | | 0.5 | 398 |
| **Al_$SnO_2$** | 600°C | 0.05 | 477 |
| | | 0.1 | 482 |
| | | 0.25 | 453 |
| | | 0.5 | 445 |
| | 900°C | 0.05 | 470 |
| | | 0.1 | 443 |
| | | 0.25 | 423 |
| | | 0.5 | 418 |
| **$TiO_2$** | 600°C | 0.05 | 350 |
| | | 0.1 | 280 |
| | | 0.25 | 212 |
| | | 0.5 | 179 |
| **ZSM-5** | nc | 0.05 | 680 |
| | | 0.1 | 839 |
| | | 0.25 | 784 |
| | | 0.5 | 856 |

### *Determination of the breakthrough of $Ge^{+4}$*

Using the experimental parameters (acid concentration and calcination temperature) determined under static experimental conditions, the breakthrough of the $Ge^{+4}$ capacity of inorganic adsorbent under dynamic (column) experimental conditions was examined. The breakthrough of $Ge^{+4}$ was calculated by Ge analysis in the eluate. The results of the test performed under dynamic conditions are given in Table 6. The amount (nanogram) of Ge in the eluate from 'ZSM-5', 'Al_$SnO_2$_900', and '$TiO_2$' samples is higher than other column-filling materials. Among other samples, the lowest breakthrough of $Ge^{4+}$ was in the 'Kw_$SnO_2$' samples.

**Table 6.** The breakthrough of $Ge^{4+}$ in the eluate solutions.

| Column-filling materials | The amount of column-filling materials (gram) | The amount of spiked Ge (ppm) | The amount of Ge (ng) In eluate |
|---|---|---|---|
| Al_$SnO_2$_900 | 2.0 | 10.159 | 44.522 |
| Kw_$SnO_2$_600 | 2.0 | 10.367 | 4.117 |
| Kw_$SnO_2$_900 | 2.0 | 11.140 | 4.035 |
| $TiO_2$_600 | 1.3 | 9.962 | 57.760 |
| ZSM-5 | 1.5 | 9.968 | 43.617 |

### *Determination of radiation stability of column and column-filling materials*

Since the column and column filling materials prepared for use in the $^{68}Ge/^{68}Ga$ generator are exposed to radiation throughout the shelf life of the generator, their radiation stability must be investigated. Based on calculations using the FLUKA MonteCarlo code, the estimated quantity of activity and its spatial distribution were determined. PP columns with dimensions of 5x0.8x1.0 cm were used as the basis for the calculations. It was calculated that the absorbed dose resulting from 1.85 GBq (50 mCi) $^{68}Ge$ loading corresponded to approximately 2 MGy. For this purpose, the column and all inorganic adsorbents used in the study were irradiated in the NÜKEN Gamma Irradiation Facility. Due to the low dose rate in the gamma irradiation facility and time constraints, these studies were limited to a total dose of 1000 kGy (2 kGy/hour). In Fig. 3, the FTIR spectrum of the column indicates that it was resistant to the applied total dose. Only a small amount of hardening of the colon was detected as a result of radiation. Radiation damages the cross-links in the material in Ge/Ga generators, causing it to harden (Han, et al., 2004). The structure and properties of all irradiated inorganic adsorbents will be compared with their non-irradiated counterparts in the 'Characterization of inorganic adsorbents' section.

### *Characterization of inorganic adsorbents*

BET analysis was performed to investigate the surface area, pore size, and pore size distribution (nano, meso, and macro) of the laboratory-synthesized and commercially available column-filling materials. BET results, which based on the physical adsorption of a nitrogen gas on the surface of the solids, indicated that all of the column-filling materials have a mesoporous structure. The particle size and surface area decreased at high calcination temperatures. Since the space between the particles decreased with the increase in temperature, uniform stacking occurred between the particles. This uniform stacking in the crystal structure explains the decrease in volume and BET area. It plays an important role in radiochemical separation. The holes in the crystal structure reduce the interaction of $Ge^{4+}$ and $Ga^{3+}$ ions, resulting in low adsorption behavior. The BET surface areas of all $SnO_2$ and $TiO_2$ decrease as the calcination temperature increases.

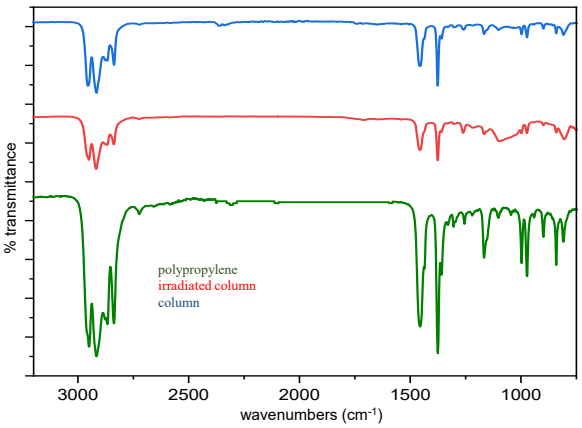


**Figure 3.** FTIR peaks of the column.

Due to the cage structure of ZSM-5, it has a high surface area of 341.95 $m^2/g$ (Table 7).

All of the irradiated inorganic adsorbents' crystal and molecular structures were compared to their non-irradiated forms using Raman spectroscopy, and XRD.

**Table 7.** The results of BET analysis.

| Sample | BET Area | Average Pore Size | Total Volume cc/g |
|---|---|---|---|
| | $m^2/g$ | Å | |
| Gl_$SnO_2$_600 | 5.61 | 19.84 | 2.78E-03 |
| Gl_$SnO_2$_900 | 2.77 | 19.49 | 1.35E-03 |
| Kw_$SnO_2$_nc | 144.90 | 20.47 | 6.38E-02 |
| Kw_$SnO_2$_600 | 21.39 | 19.97 | 1.07E-02 |
| Kw_$SnO_2$_900 | 8.37 | 19.45 | 4.07E-03 |
| Al_$SnO_2$_nc | 8.91 | 20.22 | 4.51E-03 |
| Al_$SnO_2$_600 | 8.77 | 20.10 | 4.41E-03 |
| Al_$SnO_2$_900 | 8.29 | 20.17 | 4.18E-03 |
| $TiO_2$_nc | 59.18 | 19.85 | 2.94E-02 |
| $TiO_2$_600 | 44.30 | 19.94 | 2.21E-02 |
| $TiO_2$_900 | 3.93 | 19.23 | 1.89E-03 |
| ZSM-5 | 341.95 | 20.77 | 1.41E-01 |

XRD was used to determine details about the crystal structure of the materials. Diffraction patterns of 'Gl_$SnO_2$', 'Al_$SnO_2$', and 'Kw_$SnO_2$' samples were compared with the JCPDS-01-0657 card. The effects of different calcination temperatures on the crystal structure of the sample are shown in Fig. 4. [12,16]. The first visible difference is that sharper peaks were as the calcination temperature increased in the 'Kw_$SnO_2$' samples. This indicates that the crystallinity of the inorganic adsorbent increases with the increase in calcination temperature [17]. This increase also explains the decrease in the BET area (Table 7). When compared to their non-irradiated forms, the crystal structures of all irradiated inorganic adsorbents showed no change.

In Fig. 5, the FT-IR spectra of the laboratory-synthesized and commercially available $SnO_2$ at different calcination temperatures (600°C and 900°C)

show that as the calcination temperature increases, the peaks at approximately 620 and 540 $cm^{-1}$ become stronger and weaker, respectively. The broad peaks observed around 1630 $cm^{-1}$ in the FTIR spectra of Kw_$SnO_2$ belong to the O-H bending vibration. The hydroxyl group in the surface water was thought to be responsible for these bands. The A2g, A1g, and B2g Raman active modes of another $SnO_2$, are in the ranges of 800-780 $cm^{-1}$, 650-650 $cm^{-1}$ and 490-470 cm-1, respectively. $A_{1g}$ and $B_{2g}$ modes are related to the stretching and contraction vibration modes of Sn-O bonds. The broad peaks at 1600–1400 $cm^{-1}$ of the Gl_$SnO_2$_600 and Gl_$SnO_2$_900 samples originate from glucose, and the intensity of these peaks decreases with the calcination temperature due to the fact that high temperature caused the breakdown of glucose. The peak in the range of 1200–1100 $cm^{-1}$ observed in the Kw_$SnO_2$_nc sample is due to the hydrate form of $SnO_2$ (Fig. 4) [18].

In Fig. 6, commercially purchased titanium oxide is in the anatase form (JCPDS 21-1272), and it turned into the rutile form (JCPDS 21-1276) when calcined at 900 °C. It is clear from this figure that $TiO_2$ calcined at 600 °C has a mixture of both anatase and rutile phase structure [19]).

The peaks in the Raman spectrum of $TiO_2$ as a result of different calcination temperatures are at 400-700 $cm^{-1}$ and they are related to Ti-O stretching and

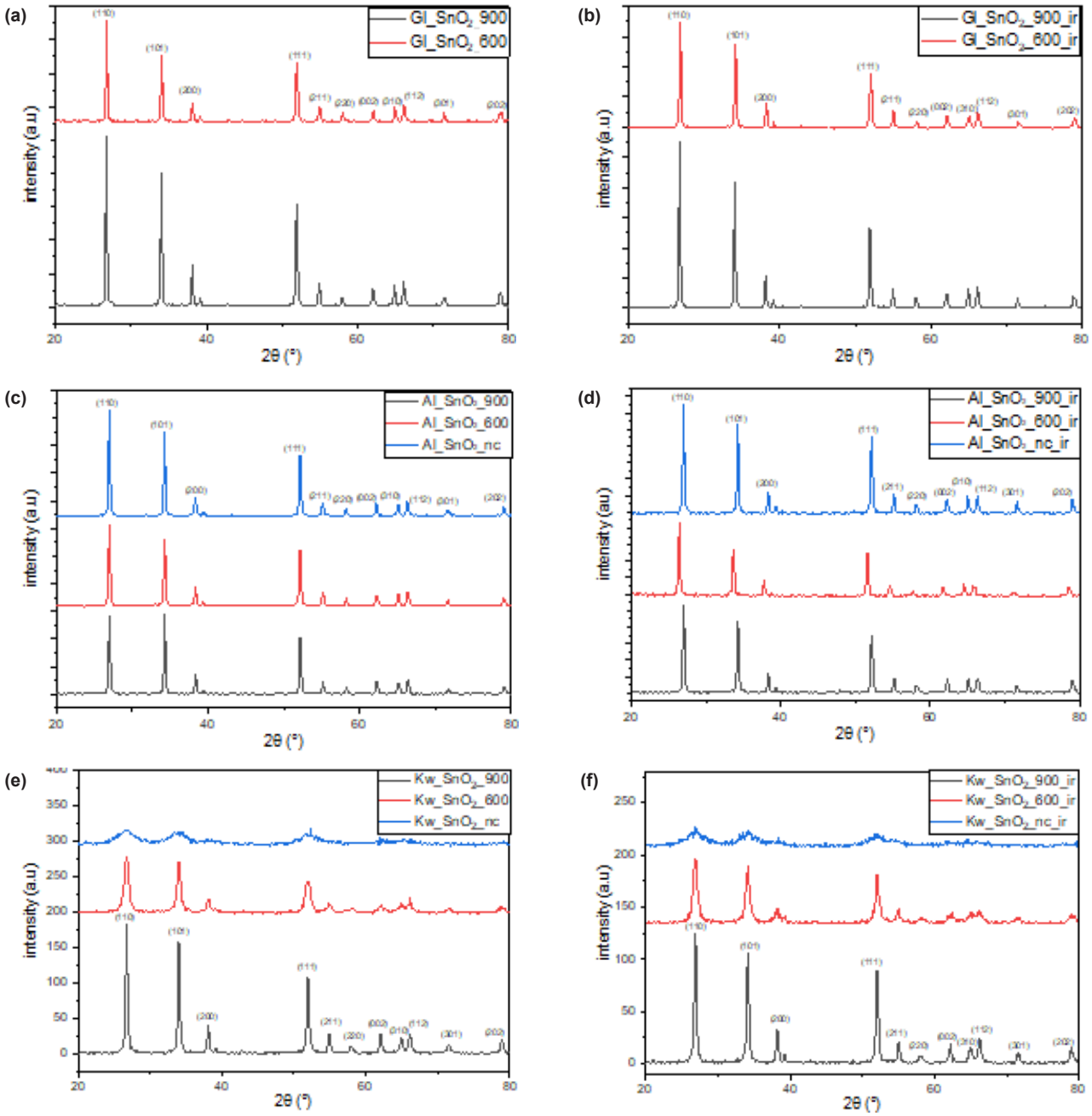


**Figure 4.** Diffraction patterns of non-irradiated (a,c,e) and irradiated (b,d,f) for "Gl_$SnO_2$", "Al_$SnO_2$" and "Kw_$SnO_2$" samples.

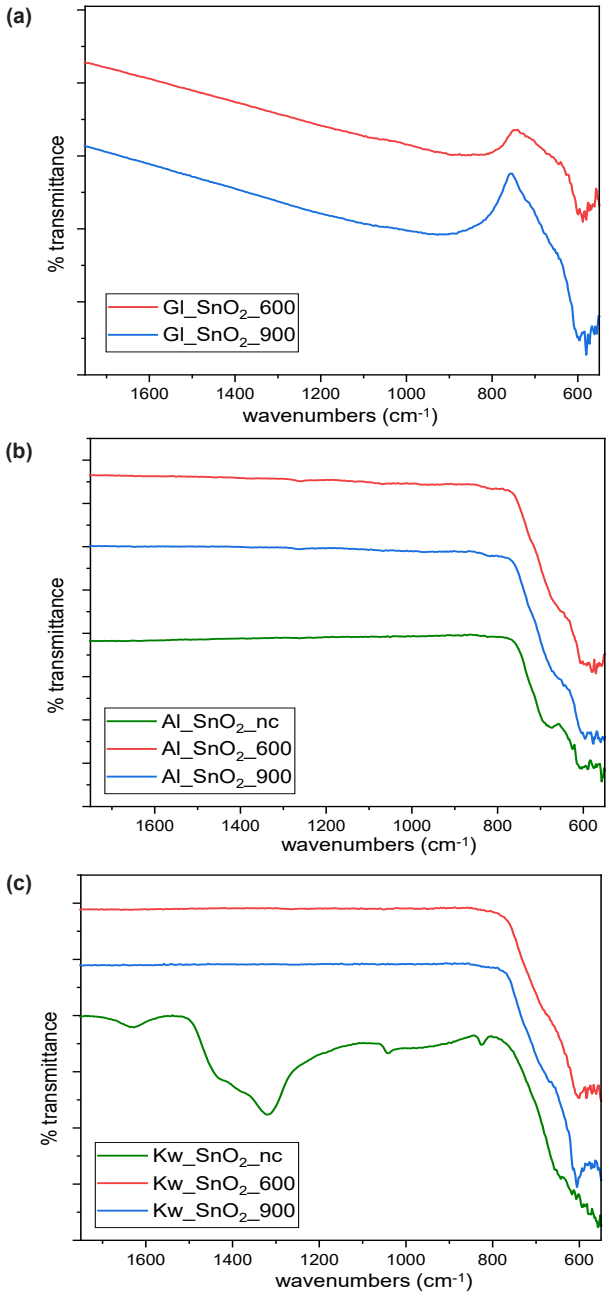


**Figure 5.** FTIR spectra of the $SnO_2$ sample a) Gl_$SnO_2$ b) Al_$SnO_2$ c) Kw_$SnO_2$ at different calcination temperature.

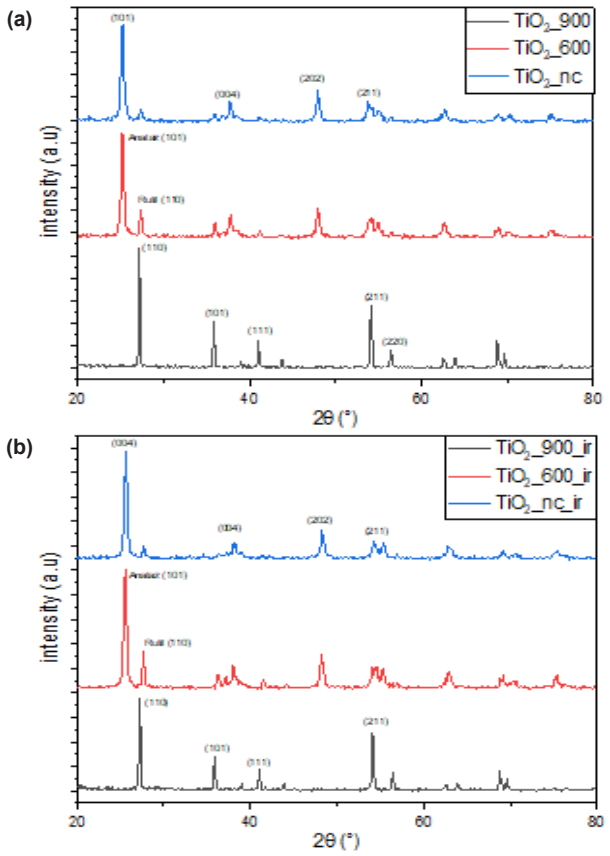


**Figure 6.** Diffraction patterns of non-irradiated (a) and irradiated (b) $TiO_2$ sampless.

Ti-O-Ti bridge modes. $TiO_2$ ($TiO_2$_nc) in anatase form has three characteristic Raman active modes at 400, 520 and 648 $cm^{-1}$ (B1g, A1g, and Eg symmetries), respectively [20]. On the other hand, $TiO_2$ calcined at 900 °C ($TiO_2$_900), which was in rutile form, exhibited characteristic stress peaks at 450 and 610 $cm^{-1}$, corresponding to Eg and A1g symmetries, respectively (Fig. 7) [21].

## 4. Conclusion

In this study, $SnO_2$ prepared by mechanochemical synthesis and commercially available inorganic adsorbents ($TiO_2$, $SnO_2$, and zeolite) as column-filling materials in the $^{68}$Ge-$^{68}$Ga generator were investigated. The calcination process was conducted to these column-filling materials at two different temperatures. Their adsorption behaviors were examined, and they were characterized using different techniques. The process of calcination increases the crystallinity and purity of column-filling materials, and affects the distribution coefficients of Ge and Ga, adsorption capacity, and the breakthrough of $Ge^{4+}$.

The distribution ratio of a radionuclide determines its retention in a column filling material. The parent and daughter radionuclides have different retention affinities for the inorganic adsorbent as a result of the difference in their $K_d$ values, which allows for their efficient separation. Generally, the parent radioisotope has a very high $K_d$ value, and that of the daughter radioisotope is negligibly small. The distribution coefficients of Ge and Ga were determined in static experiments using different concentrations of HCl (0.01-1.5 M). These inorganic adsorbents with the highest distribution coefficient of $^{68}$Ge and lower $^{68}$Ga are Kw_$SnO_2$_600, Kw_$SnO_2$_900, Al_$SnO_2$_600, Al_$SnO_2$_900, $TiO_2$ and ZSM-5. These inorganic adsorbents with better $K_d$ of Ge and lower $K_d$ of Ga values were subsequently evaluated for their sorption capacity. It is noted that the large difference between the distribution coefficients of Ge and Ga affects the radiochemical separation efficiency. Under static experimental conditions, the qe of $Ge^{4+}$ of each of these inorganic adsorbents was calculated at different concentrations of HCl (0.05-0.5 M). It gave information

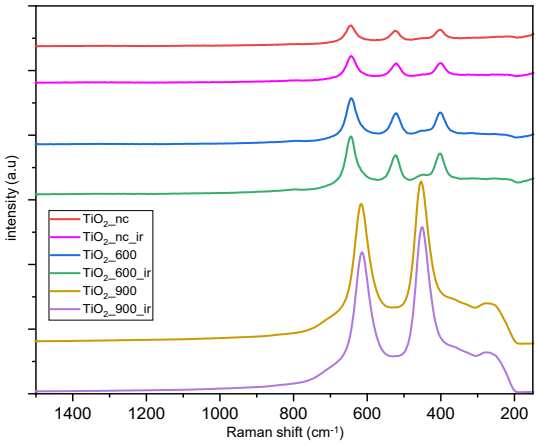


**Figure 7.** Raman spectrum of irradiated and non-irradiated $TiO_2$ sample at different calcination temperatures.

about how 1 gram of column-filling materials absorbs how many micrograms of Ge. While the maximum adsorption of $Ge^{4+}$ and elution of $Ga^{3+}$ in ZSM-5 and $TiO_2$ samples occurs at 0.1 M HCl, 0.5 M HCl is required for $SnO_2$. The breakthrough of $Ge^{4+}$ in five different column-filling materials was examined under dynamic experimental conditions by establishing a column setup. According to the results, 'Kw_$SnO_2$_900', which has a high $Ge^{4+}$ adsorption capacity, and a low breakthrough of $Ge^{4+}$ with a high $K_d$ of Ge and low $K_d$ of Ga, can be selected as column filling material to produce $^{68}Ga$ in $^{68}Ge/^{68}Ga$ generators. It is concluded that 'ZSM-5' had a high affinity for both radionuclides, and it was thought that it could be used as a molecular sieve or waste storage' in other studies, although not in generator systems. Based on these results, it can be inferred that for loading Ge into the generator column containing Kw_$SnO_2$_900, the molarity of the feed solution should be 0.5 to achieve a high adsorption capacity.

Analyses of characterization for column-filling materials were performed with different characterization techniques (BET, XRD, FTIR, and Raman spectroscopy). These characterization studies explained the reasons why the column filling material used in the generator system has high adsorption properties. According to BET results, the pore size decreased with the applied calcination process, especially with the increase in the calcination temperature. Since the space between the particles decreased with the increase in temperature, denser stacking occurred between the particles. This frequent stacking explains the decrease in volume and BET area and is evidence that it plays an important role in the realization of radiochemical separation. It is proven that the crystallinity and crystal sizes of inorganic adsorbents increase after the calcination process. FTIR and Raman spectra provide information about their molecular structure. The calcination process leads to minor differences in all inorganic adsorbents except 'Kw_$SnO_2$' samples. The biggest visible difference is that the O-H band of the water crystal seen in the 'Kw_$SnO_2$' samples disappears thanks to the calcination process (600 ºC and 900 ºC).

Column-filling materials used in generator systems are exposed to radiation during the shelf life of the generator, and these materials must be resistant to the radioactivity that occurs during repeated elutions. The radiation resistance required for the column and all inorganic adsorbents was demonstrated in the characterization tests conducted both prior to and following irradiation. Only a small amount of hardening of the colon was detected due to the effect of radiation. All inorganic adsorbents that were exposed to radiation had the same crystal structures as their non-irradiated forms. Therefore, if a generator filled with tin oxide (Kw_$SnO_2$_900) is produced as a prototype, polyetheretherketone (PEEK) and borosilicate glass columns, which are known to have high radiation resistance, can be used instead of PP columns.

## 5. Acknowledgements

The research carried out at the Turkish Energy, Nuclear and Mineral Research Agency (TENMAK), Nuclear Energy Research Institute is a part of the studies within the scope of the dissertation and was fully supported by TENMAK.

## References

[1]. Bao, B. & Song, M.(1996). A new 68Ge/68Ga generator based on CeO2. Journal of Radioanalytical and Nuclear Chemistry. 213, p. 233–238 https://doi.org/10.1007/BF02163569

[2]. Romero, E. & Morcillo, M. A.( 2017). Inorganic oxides with potential application in the preparation of a 68Ge/68Ga generator system. Applied Radiation and Isotopes. 119, pp. 28-35. https://doi.org/10.1016/j.apradiso.2016.10.014

[3]. Rösch, F.(2013). 68Ga radiopharmaceuticals: Current status and future. s.l.:Johannes Gutenberg University. https://humanhealth.iaea.org/HHW/NuclearMedicine/Conferences/IPET2015/Presentations/Tuesday/07_Parallel_Session_1b/03_Roesch.pdf

[4]. Romero, E. et al.(2020). Development and long-term evaluation of a new 68Ge/68Ga generator based on nano-SnO2 for PET imaging. Scientific Reports. 10. https://doi.org/10.1038/s41598-020-69659-8

[5]. Saha, G. B.(2010). Fundamentals of Nuclear Pharmacy. New York: Springer. http://dx.doi.org/10.1007/978-1-4419-5860-0

[6]. Ondrák Fialová, K. et al.(2023). Preparation and Surface Characterization of Cerium Dioxide for Separation of 68Ge/68Ga and Other Medicinal Radionuclides. Materials, Volume 16. https://doi.org/10.3390/ma16051758

[7]. Neirinckx, R. D., Layne, W. W., Sawan, S. P. & Davis, M. A., (1982). Development of an ionic germanium 68 gallium 68 generator III.chelate resins as chromatographic substrates for germanium. International Journal of Applied Radiation and Isotopes. 33 (4), pp. 259-266. https://doi.org/10.1016/0020-708X(82)90024-2

[8]. Aardaneh, K. & van der Walt, T. N. (2006). Ga2O for target, solvent extraction for radiochemical separation and SnO2for the preparation of a68Ge/68Ga generator. ,Journal of Radioanalytical and Nuclear Chemistry. 268 (1), pp. 25-32. https://doi.org/10.1007/s10967-006-0118-5

[9]. Rösch, F. (2012). Past, present and future of 68Ge/68Ga generators. Applied Radiation and Isotopes. 76, pp. 24-30. 24-30. https://doi.org/10.1016/j.apradiso.2012.10.012

[10]. IAEA, (2019). Gallium-68 Cyclotron Production, Vienna: International Atomic Energy Agency. IAEA-TECDOC-1863 ¦ 978-92-0-100819-0

[11]. Chakravarty , R.(2011). s.l.:Doctoral Dissertation, Homi Bhabha National Institute.

[12]. Chakravarty, R. et al. (2016). Mechanochemical Synthesis of Mesoporous Tin Oxide: A New Generation Nanosorbent for 68Ge/68Ga Generator Technology. Dalton Transaction, pp. 45 13361-13372. https://doi.org/10.1039/C6DT01921H

[13]. Ekebas Cavdar E.(2022). Ge-Ga Jeneratöründe Kullanilacak Olan Çeşitli Kolon Dolgu Malzemelerin Sentezi, Karakterizasyonu Ve Uygulamasi.TENMAK.

[14]. Davies, C. M.,( 2012). Determination Of Distribution Coefficients For Cation Exchange Resin And Optimisation Of Ion Exchange Chromatography For Chromıum Separation For Geological Materials. s.l.:Doctoral Dissertation. The University of Manchester.

[15]. Rzaij, J. M. & Abass, A. M. (2020). Review on TiO2 Thin Film as a Metal Oxide Gas Sensor. Journal of Chemical Reviews. 2, pp. 114-121. https://doi.org/10.33945/SAMI/JCR.2020.2.4

[16]. Karthik, T. V. K., Maldonado, A. & Olvera, M. d. l. L. (2012). Synthesis of tin oxide powders by homogeneous precipitation. Structural and morphological characterization. Electrical Engineering, Computing Science and Automatic Control (CCE), 2012 9th International Conference on. https://doi.org/10.1109/ICEEE.2012.6421145

[17]. Çetin, C. E.(2011). Mikrodalga ışınlanması ile çeşitli metal-kükürt yarı iletken nanoparçacıklarının sentezi ve karakterizasyonu. s.l.:Yüksek Lisans Tezi, Ankara Üniversitesi.

[18]. Bhardwaj, N. & Mohapatra, S. (2015). Fabrication of SnO2 three dimentional complex microcrystal chains by carbothermal reduction method. Advanced Materials Letters. 6 (2), pp. 148-152. https://doi.org/10.5185/amlett.2015.5681

[19]. Buwa, S. (2014). Production and Evaluation of a TiO2 based 68Ge/68Ga Generator. s.l., Doctoral Dissertation, University of the Western Cape.

[20]. El-sherbiny, S., Morsy, F. A., Samir, M., & Fouad, O. A. (2014). Synthesis, characterization and application of TiO2 nanopowders as special paper coating pigment. Applied Nanoscience, 305-303. https://doi.org/10.1007/s13204-013-0196-y

[21]. Challagulla, S., Tarafder, K., Ganesan, R. & Roy, S.(2017). Structure sensitive photocatalytic reduction of nitroarenes over TiO2. Scientific Reports. 7. https://doi.org/10.1038/s41598-017-08599-2